

## RED CELLS, IRON, AND ERYTHROPOIESIS

## The actin-binding protein profilin 2 is a novel regulator of iron homeostasis

Sara Lusciati,<sup>1,2</sup> Bruno Galy,<sup>3</sup> Lucia Gutierrez,<sup>4</sup> Michael Reinke,<sup>5</sup> Jorge Couso,<sup>1,2</sup> Maya Shvartsman,<sup>1</sup> Antonio Di Pascale,<sup>6</sup> Walter Witke,<sup>5</sup> Matthias W. Hentze,<sup>7</sup> Pietro Pilo-Boyl,<sup>5</sup> and Mayka Sanchez<sup>1,2</sup>

<sup>1</sup>Program of Predictive and Personalized Medicine of Cancer, Germans Trias i Pujol Research Institute, Campus Can Ruti, Badalona, Spain; <sup>2</sup>Iron Metabolism: Regulation and Diseases Group, Josep Carreras Leukaemia Research Institute, Campus ICO–Germans Trias i Pujol, Badalona, Spain; <sup>3</sup>Division of Virus-Associated Carcinogenesis, German Cancer Research Centre, Heidelberg, Germany; <sup>4</sup>Department of Biomaterials and Bioinspired Materials, Instituto de Ciencia de Materiales de Madrid, Madrid, Spain; <sup>5</sup>Institute of Genetics, University of Bonn, Bonn, Germany; <sup>6</sup>Department of Pharmacy, University of Naples Federico II, Naples, Italy; and <sup>7</sup>European Molecular Biology Laboratory, Heidelberg, Germany

## Key Points

- *Pfn2* mRNA has a functional and conserved IRE in the 3' untranslated region.
- *Pfn2* knockout mice display an iron phenotype with iron accumulation in specific areas of the brain and depletion of liver iron stores.

Cellular iron homeostasis is controlled by the iron regulatory proteins (IRPs) 1 and 2 that bind *cis*-regulatory iron-responsive elements (IRE) on target messenger RNAs (mRNA). We identified *profilin 2* (*Pfn2*) mRNA, which encodes an actin-binding protein involved in endocytosis and neurotransmitter release, as a novel IRP-interacting transcript, and studied its role in iron metabolism. A combination of electrophoretic mobility shift assay experiments and bioinformatic analyses led to the identification of an atypical and conserved IRE in the 3' untranslated region of *Pfn2* mRNA. *Pfn2* mRNA levels were significantly reduced in duodenal samples from mice with intestinal IRP ablation, suggesting that IRPs exert a positive effect on *Pfn2* mRNA expression *in vivo*. Overexpression of *Pfn2* in HeLa and Hepa1-6 cells reduced their metabolically active iron pool. Importantly, *Pfn2*-deficient mice showed iron accumulation in discrete areas of the brain (olfactory bulb, hippocampus, and midbrain) and reduction of the hepatic iron

store without anemia. Despite low liver iron levels, hepatic hepcidin expression remained high, likely because of compensatory activation of *hepcidin* by mild inflammation. Splenic ferroportin was increased probably to sustain hematopoiesis. Overall, our results indicate that *Pfn2* expression is controlled by the IRPs *in vivo* and that *Pfn2* contributes to maintaining iron homeostasis in cell lines and mice. (*Blood*. 2017;130(17):1934-1945)

## Introduction

Cellular iron metabolism is maintained posttranscriptionally by iron regulatory proteins (IRP) 1 and 2, which bind conserved RNA stem-loop structures named iron-responsive element (IRE).<sup>1</sup> IRPs bind to IREs present in messenger RNAs (mRNAs) that encode proteins involved in iron acquisition (transferrin receptor 1, Tfr1, also known as *Tfrc*; divalent metal transporter 1, Dmt1, also known as *Slc11a2*), storage (ferritin H, Fth1; ferritin L, Ftl), utilization (erythroid 5-aminolevulinic acid synthase, Alas2; mitochondrial aconitase, Aco2), export (ferroportin, Fpn, also known as *Slc40a1*), and iron/oxygen sensing (hypoxia-inducible factor 2- $\alpha$ , Hif2 $\alpha$ , also known as *EPAS1*).<sup>2-5</sup>

Functional IREs present a small asymmetrical cytosine bulge on the 5' strand of the stem and a 6-nucleotide apical loop with the sequence 5'-CAGWGH-3' (W = adenosine or uridine and H = adenosine, cytosine, or uridine). The first cytosine and the fifth guanosine are pairing, forming an AGW pseudotriple loop. The IRP1-IRE crystal structure revealed that the C-bulge and the pseudotriple loop residues are important protein contact points.<sup>6</sup> The IRE upper stem consists of 5 paired nucleotides with or without the presence of an extra unpaired uridine residue downstream of the apical loop (*Slc11a2* and *Epas1* IREs), whereas the lower stem is of variable length.<sup>7,8</sup>

IRP binding to IREs is regulated by intracellular iron levels as well as by nitric oxide, oxidative stress, and hypoxia. IRP activity is high in iron-deficient cells and low in iron-replete conditions. Both IRPs inhibit translation when bound to an IRE located in the 5' untranslated region (UTR), whereas their association with *Tfrc* 3' UTR IREs prevents mRNA degradation.<sup>7-9</sup>

Combined, body-wide ablation of both IRP1 and 2 in mice is embryonically lethal, showing that the IRP/IRE system is essential.<sup>10,11</sup> Tissue-specific coablation of both proteins also revealed important functions of the IRPs in the intestine,<sup>12,13</sup> in the liver,<sup>14</sup> as well as in macrophage-mediated immunity.<sup>15</sup> On the other hand, excessive accumulation of IRP2 seemed lethal in mice,<sup>16</sup> whereas a moderate gain of IRP1 function due to expression of a constitutively active *Irp1* transgene resulted in macrocytic erythropenia associated with impaired erythroid differentiation.<sup>17</sup> A key, yet unresolved question is whether all biological functions of IRP1 and/or IRP2 are achieved through regulation of the currently known IRE-containing genes, or whether there are other targets. We recently determined the IRP/IRE regulatory repertoire on a transcriptome-wide scale and identified novel mRNAs that bind to both IRPs,<sup>18</sup> including *profilin 2* (*Pfn2*).

Submitted 30 November 2016; accepted 30 July 2017. Prepublished online as *Blood* First Edition paper, 3 August 2017; DOI 10.1182/blood-2016-11-754382.

The online version of this article contains a data supplement.

The publication costs of this article were defrayed in part by page charge payment. Therefore, and solely to indicate this fact, this article is hereby marked "advertisement" in accordance with 18 USC section 1734.

© 2017 by The American Society of Hematology

Profilins constitute a family of small monomeric actin-binding proteins containing an actin-binding domain, a poly-L-proline-binding domain, and a phosphatidylinositol bisphosphate-binding domain.<sup>19</sup> In mammals, 4 different profilin genes have been identified (*Pfn1*, *Pfn2*, *Pfn3*, and *Pfn4*) with Pfn2 being predominantly expressed in the central nervous system. In mouse brain, Pfn2 interacts with vesicle and membrane trafficking proteins such as dynamin 1 (Dnm1), a multimeric GTPase required for receptor-mediated endocytosis.<sup>20,21</sup> Pfn2 binds with high affinity to Dnm1, resulting in its sequestration and thereby inhibiting endocytosis in neurons.<sup>22,23</sup> Pfn2 ablation in mice results in viable rodents born with the expected Mendelian ratio, although ~20% of the mutant pups do not reach weaning age, possibly because of behavioral deficits (P.P.B., unpublished observations). Compared with control, Pfn2-null animals are hyperreactive and show increased locomotion and exploratory behavior. This phenotype correlates with greater synaptic excitability and increased neurotransmitter release in glutamatergic neurons of the cortico-striatal pathway, because of higher probability of synaptic vesicle exocytosis<sup>24</sup>; therefore, Pfn2 appears to also negatively regulate vesicle exocytosis.<sup>24</sup>

In this work, we report the identification of a conserved IRE in the 3' UTR of the *Pfn2* mRNA and provide evidence that Pfn2 expression is modulated in vivo by the IRPs. We show that Pfn2 knockout (KO) mice have a hitherto unnoticed iron phenotype, with accumulation of the metal in specific areas of the brain and a concomitant depletion of liver iron stores. This study uncovers a novel player in the IRP/IRE regulatory system and unveils the previously unrecognized importance of Pfn2 for iron homeostasis.

## Methods

### Animals

Mice were kept on a constant 12-hour light/dark cycle, and food and water were supplied ad libitum. Male wild-type (WT) and *Pfn2*<sup>-/-</sup> littermates<sup>24</sup> on a C57Bl6/N genetic background were euthanized at 7 to 9 months of age by cervical dislocation, and dissected tissues were flash-frozen in liquid nitrogen for RNA, protein, and iron quantification studies. For histological analysis, mice were anesthetized with ketamine and xylazine (1 and 0.1 mg per 10 g of body weight, intraperitoneally, respectively; Sigma-Aldrich) and subjected to transcardial perfusion. For hematological and biochemical studies, heparinized or EDTA blood was collected from tail vein or via cheek-bleeding. Bone marrow was flushed out from femur and tibia bones. All experiments were performed according to EU regulations (license nos. 19/2005-B and AZ 84-02.04.2013. A233).

### Cell culture

HeLa and Hepa1-6 cells lines were obtained from ATCC (Wesel, Germany). Culture and transfection conditions for all cells used in the study are described in the supplemental Data, available on the *Blood* Web site.

### Plasmid construction

Plasmids (I-12.CATwt and mut) for the synthesis of human *FTH1*-IRE probes for electrophoretic mobility shift assay (EMSA) were previously described.<sup>25</sup> Mouse and human *Pfn2* IRE sequences (WT or  $\Delta A$  mutated) were subcloned into the I-12.CAT plasmid by replacement of the WT *FTH1*-IRE sequence using annealed synthetic oligonucleotides. A mouse *Pfn2* full-length complementary DNA clone was purchased from OriGene Technologies. Fragments A-E in *Pfn2* 3' UTR were amplified by polymerase chain reaction and cloned into pCMV-XL5 (OriGene Technologies) using *EcoRI* and *HindIII* restriction sites. The mutated fragment A was obtained by site-directed mutagenesis (Stratagene). Pfn2-Mut S138D plasmid was previously described.<sup>23</sup> Primers used for cloning are listed in supplemental Table 1.

### Nonradioactive competitive EMSA

Competitive EMSAs were performed as previously described<sup>3,26-28</sup> (see supplemental Data).

### RNA

Protocols for isolation of total RNA, reverse transcription, and quantitative polymerase chain reaction (qPCR) were described previously.<sup>18,26</sup> Expression levels of housekeeping mRNAs (*RPL19*, *Tbp*, and  $\beta$ -*actin*) were used as calibration controls. Sequences for qPCR primers are listed in supplemental Table 1.

### Labile iron pool assay and reactive oxygen species detection

The cytosolic labile iron pool (LIP) and reactive oxygen species (ROS) levels were measured by the fluorescent Calcein-AM method and the dichlorofluorescein assay, respectively, as previously described.<sup>29,30</sup> Details for both assays are provided in the supplemental Data.

### Plasma IL-6 cytokine analysis

Whole blood was collected in EDTA tubes and centrifuged at 1500g for 15 minutes at 4°C. Plasma supernatants were aliquoted and frozen in liquid nitrogen. Plasma samples were diluted 1:2 in assay buffer and measured using the Mouse Angiogenesis/Growth Factor Magnetic Bead Kit for detection of interleukin-6 (IL-6; EMD Millipore; MAGPMAG-24K) together with xMAP platform (EMD Millipore) according to the manufacturer's instructions. The data were analyzed with the MILLIPIX Analyst Software.

### Tissue iron content

Liver, duodenum, spleen, kidney, lung, heart, and skeletal muscle non-heme iron content was measured using the previously described bathophenanthroline colorimetric method.<sup>31,32</sup> Total iron content of brain areas and bone marrow was determined by atomic absorption spectrometry as previously described.<sup>33</sup> Further details are described in the supplemental Data.

### Perls Prussian non-heme iron histochemistry

Nine- to 11-month-old mice were used for histological staining of non-heme iron using the perfusion Perls method with 3,3'-diaminobenzidine intensification as described.<sup>34,35</sup> A detailed protocol can be found in the supplemental Data.

### Total protein extraction and immunoblotting

Mouse tissues were lysed on ice in 44 mM Tris/HCl pH 6.8, 8% glycerol, 1.5% sodium dodecyl sulfate, 3.2% b-mercaptoethanol, 0.12% wt/vol bromophenol blue using a Potter-Elvehjem homogenizer with a polytetrafluoroethylene pestle at 600 rpm. Samples were then incubated for 10 minutes at 99°C (for ferroportin detection, the heat denaturation step was omitted). Total protein concentration was determined using the Pierce BCA Protein Assay kit (Thermo Scientific) or the BioRad Bradford reagent following the manufacturer's instructions. For details, see supplemental Data.

### Statistics

Data are shown as mean values  $\pm$  standard error of the mean unless otherwise indicated. Statistical analysis was performed using 2-tailed Student *t* test if 2 groups were compared, or 1-way analysis of variance test with Bonferroni multiple comparison post-hoc test if 3 or more groups were compared. *P* values are reported as follows: \* $0.01 < P \leq .05$ , \*\* $0.001 < P \leq .01$ , \*\*\* $P \leq .001$ . Statistical analysis of Affymetrix microarrays was performed using a moderated Student *t* test with Linear Models for Microarray Data,<sup>36</sup> and *P* value was adjusted for multiple comparisons with FDR.<sup>37</sup>

Supplemental Data details the microarray analysis, transmission electron microscopy (TEM), and energy dispersive X-ray spectroscopy (EDS) measurements.

## Results

### Identification of *Pfn2* as a novel IRP binding mRNA with a conserved 3' UTR IRE

We have previously identified novel mRNAs that interact with IRP1 and/or IRP2 by combining immunoprecipitation and microarray analysis.<sup>18,38</sup> Three independent Affymetrix probes identified *Pfn2* as a mRNA associated with both IRPs in several mouse tissues.

Although bioinformatics predictive tools such as the SIREs algorithm<sup>39</sup> fail to recognize a canonical IRE motif in the *Pfn2* transcript, the *Pfn2* mRNA was enriched in a pull-down assay using recombinant IRP1 and RNA extracted from mouse spleen, brain, or liver (2.4- to 11.4-fold enrichment of *Pfn2* mRNA, depending on tissue; supplemental Figure 1). Furthermore, a full-length *Pfn2* transcript could displace the interaction between recombinant IRP1 and a *ferritin H* IRE probe in a competitive EMSA, whereas a *Pfn2* transcript with most of its 3' UTR deleted could not (Figure 1C). These results indicate that *Pfn2* mRNA interacts with IRP1 through an element located within its 3' UTR.<sup>18</sup>

To delineate the exact position of this element, we subcloned and tested 5 overlapping 250-bp fragments of the *Pfn2* mRNA 3' UTR (Figure 1A) in competitive EMSAs using recombinant IRP1 (Figure 1C) or IRP2 (supplemental Figure 3A). We found that the interaction between *Pfn2* mRNA and the IRPs was mediated by the most upstream region (fragment A) of the *Pfn2* mRNA 3' UTR (Figure 1C; supplemental Figure 3). A detailed mRNA folding analysis identified a noncanonical IRE motif 326 bp downstream of the stop codon (Figure 1B). The *Pfn2* IRE motif is conserved across several mammalian species (Figure 1E; supplemental Figure 2), and similarly to other IREs, consists of a 5-paired upper stem and a midstem C bulge (C8; Figure 1B), but differs from a canonical motif by the sequence of the hexanucleotide apical loop (AAGUUG instead of CAGUGH). Nonetheless, the first and the fifth ribonucleotide (adenosine and uridine) can pair, allowing the formation of an AGU pseudotriple loop (Figure 1B), and deletion of the first adenosine in the apical loop (AAGUUG; Figure 1B) of the mouse and human *Pfn2* IREs abrogates binding to IRP1 and IRP2, as assessed by competitive EMSA (Figure 1D; supplemental Figure 3). We also demonstrated that the IRP-IRE competitive binding is dose dependent for *Pfn2* mRNA (supplemental Figure 3B). Of note, 2 isoforms of the mouse *Pfn2* mRNA have been described.<sup>40</sup> These splice variants differ in the first 267 bp of the last exon and yield 2 proteins with different C-terminal amino-acid composition,<sup>40,41</sup> but both retain the 3'-IRE motif.

Altogether, these results reveal the presence of a conserved IRE in the 3' UTR of *Pfn2* mRNA bound by both IRP1 and IRP2.

### Modulation of *Pfn2* expression by IRPs

The *Tfrc* mRNA, which contains 5 IREs in its 3' UTR, is stabilized upon IRP binding in iron-deficient cells and is conversely degraded in iron-replete conditions when IRP activity is low. We therefore tested whether *Pfn2* mRNA expression is regulated by iron in 4 different cell lines (NIH3T3, RAW264, Hepa1-6, and AML12). Contrasting with *Tfrc*, *Pfn2* transcript levels did not increase upon iron chelation with deferoxamine (DFO), as assessed by qPCR; we even observed a significant reduction of *Pfn2* mRNA levels in Hepa1-6 cells (supplemental Figure 4A, *Pfn2*). *Pfn2* mRNA expression was nonetheless reduced in Hepa1-6 cells upon iron loading with hemin (supplemental Figure 4A, *Pfn2*). A time course experiment in Hepa1-6 cell lines showed that *Pfn2* mRNA levels were significantly and constantly decreased after 5, 10, 15, and 20 hours of hemin treatment, similarly to the *Tfrc* mRNA,

whereas *Pfn2* mRNA reduction after DFO treatment was only transient (supplemental Figure 4B). Because IRE activity can be context dependent<sup>12</sup> and the regulation of *Pfn2* via its 3' UTR IRE may not be recapitulated in cultured cell lines, we also tested if *Pfn2* mRNA expression was modulated in C57BL/6 mice fed with a low-iron diet. *Tfrc* mRNA expression was expectedly increased in the liver, duodenum, and spleen of iron-deficient mice, but *Pfn2* mRNA remained unchanged (supplemental Figure 5). Hence, iron depletion alone seems not to suffice to stimulate *Pfn2* mRNA expression neither in cultured cells nor in mice, at least under the experimental conditions tested.

We therefore took advantage of a mouse model with acute loss of IRP1 and IRP2 function in the intestinal mucosa to study the impact of the IRPs on *Pfn2* expression *in vivo*.<sup>12</sup> As expected, *Tfrc* mRNA levels were reduced by ~50% (Figure 2). Importantly, *Pfn2* mRNA levels were also significantly decreased (25%). These results thus indicate that IRPs exert a positive effect on *Pfn2* mRNA expression, as expected for a 3' UTR IRE-containing transcript.

### *Pfn2* regulates the cLIP of the cell

Because *Pfn2* is regulated by the IRPs, the key regulators of iron metabolism in the cell, we next studied the influence of *Pfn2* on cellular iron metabolism. Ectopic overexpression of WT *Pfn2* in HeLa cells was previously reported to inhibit endocytosis, thereby blocking transferrin uptake. This effect was not observed with a mutant *Pfn2* form (*Pfn2*-Mut S138D) that binds actin but not dynamin 1.<sup>23</sup>

To further study the effect of *Pfn2* on cellular iron levels, we transiently overexpressed either the WT or the mutated (mut S138D) form of *Pfn2* in HeLa cells and measured the cytoplasmic labile iron pool (cLIP). Overexpression of both clones was at similar levels (data not shown). As control, cells were either transfected with mouse *ferritin H* (*Fth1*) or treated with DFO to chelate iron and thus reduce the cLIP; conversely, they were treated with ferric ammonium citrate to increase the cLIP.

We found that overexpression of WT *Pfn2* reduced the LIP as efficiently as *Fth1* or DFO treatment, whereas overexpression of the S138D *Pfn2* mutant had no effect (Figure 3A). Similar results were obtained in HeLa and Hepa1-6 cells stably overexpressing *Pfn2* vs *Pfn2*-Mut S138D (Figure 3B). To further demonstrate that *Pfn2* reduces cellular iron availability, we measured ROS levels in H<sub>2</sub>O<sub>2</sub>-treated cells. We found that transient WT *Pfn2* expression reduced ROS levels in H<sub>2</sub>O<sub>2</sub>-treated HeLa cells, and that overexpression of *Pfn2*-Mut S138D has no effect on ROS (Figure 3C). These data demonstrate that *Pfn2* decreases the metabolically active iron pool in the cell.

### Abnormal iron distribution in *Pfn2*-deficient mice

*Pfn2*<sup>-/-</sup> mice have been reported to have neuronal hyperexcitability because of increased synaptic vesicle exocytosis.<sup>24</sup> However, the role of *Pfn2* in iron metabolism has not been addressed. In light of our finding that *Pfn2* influences iron metabolism in cultured cells, we next studied the role of *Pfn2* in iron metabolism *in vivo* in *Pfn2*-null mice.

Enhanced Prussian blue staining of iron with the Perls perfusion method was performed in key organs of iron homeostasis, including the duodenum (site of iron absorption), the liver (site of iron storage), the spleen (site of iron recycling), and the bone marrow (site of iron utilization). We also analyzed the brain and kidney because of high *Pfn2* expression in those tissues. We did not observe any change in the amount and distribution of iron in the duodenum, spleen, bone marrow, and kidney of *Pfn2*-deficient mice (data not shown). This observation was confirmed by quantification of total non-heme iron levels in duodenum, spleen, and kidney with the bathophenanthroline chromogen method (Figure 4C), and in the bone marrow by atomic absorption

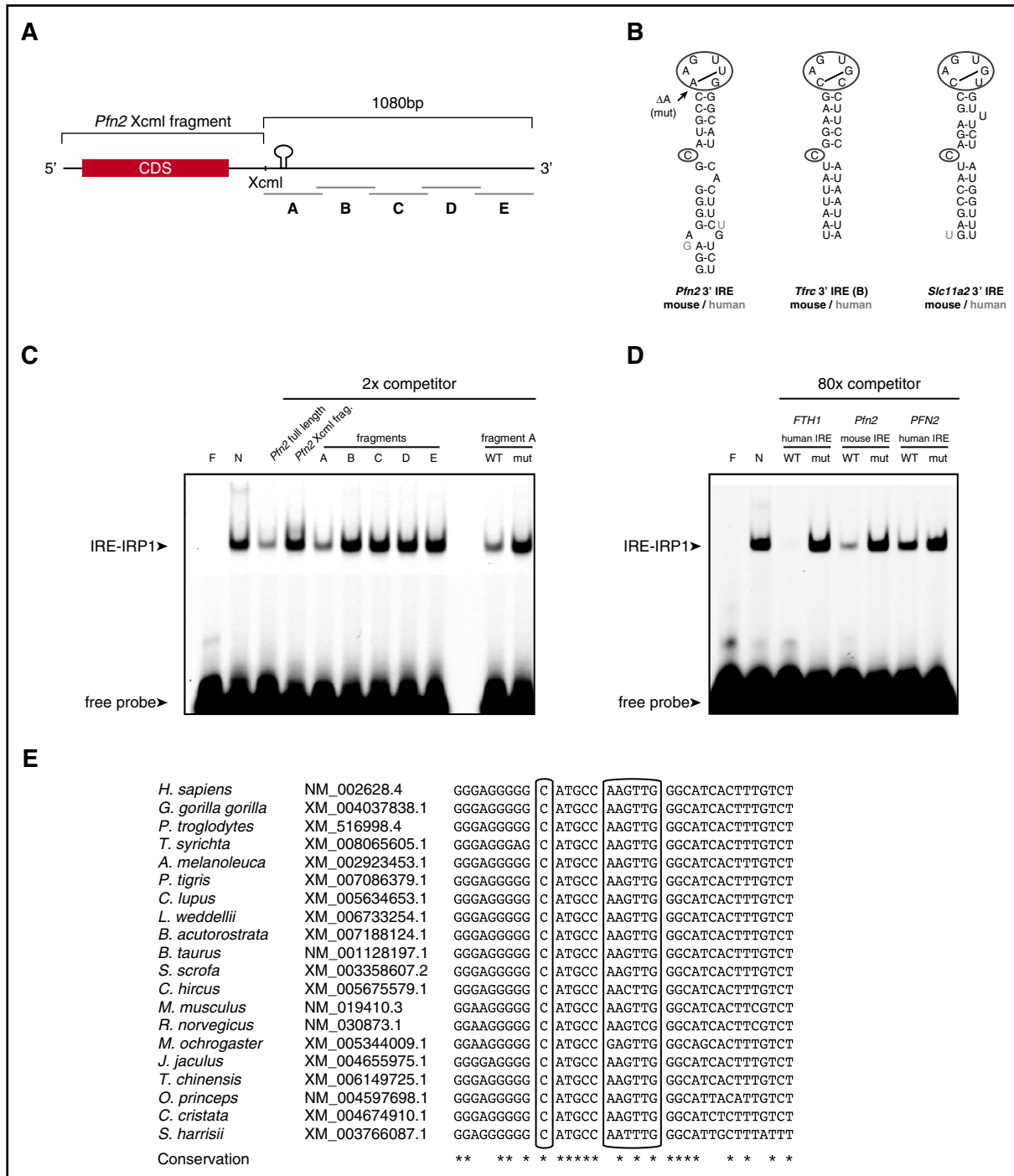


**Figure 1. Identification of the *Pfn2* 3' UTR IRE and IRP binding studies.** (A) Schematic representation of the *Pfn2* mRNA. Coding region (black box), *Pfn2* XcmI fragment, and fragments A to E and IRE are shown. (B) Human and mouse 3' IRE motifs in *Pfn2*, *Tfrc*, and *Slc11a2* mRNAs. Notice differences in sequence in the apical loop. The arrow indicates the deletion of the adenosine ( $\Delta A$ , mut) used as mutant construct. (C) Nonradioactive competitive EMSA using fluorescent *ferritin H* IRE-labeled probe and twofold molar excess of unlabeled competitors (full-length *Pfn2* mRNA or *Pfn2* mRNA fragments). Constructs or fragments (XcmI fragment, A to E fragment) used as competitors are indicated. Mut, fragment A containing a single deletion in the first A of the 6-nucleotides apical loop; WT, wild-type fragment A. One representative experiment out of 4 is shown. (D) Nonradioactive competitive EMSA using fluorescent *ferritin H* IRE-labeled probe and 80-fold molar excess of unlabeled competitors (*ferritin H* or mouse and human *Pfn2* IRE sequences). (E) Representative phylogenetic conservation of the *Pfn2* IRE among mammals; an extended alignment is shown in supplemental Figure 2. Asterisks (\*) indicate residues conserved in all aligned species. CDS, coding sequence.

spectrometry measurement of total iron (Figure 4D). Hence, Pfn2 seems dispensable for maintaining iron homeostasis in the intestine, spleen, kidney, and bone marrow of mice kept under standard laboratory conditions. Interestingly, iron deposits were observed in particular brain areas such as the Ammon horn of the hippocampus (Figure 4A). The

analysis of dissected brain tissue by atomic absorption spectrometry confirmed the accumulation of iron in the hippocampus but also in the olfactory bulb and the midbrain of *Pfn2*<sup>-/-</sup> mice (Figure 4E). Contrasting with iron loading of neurons, liver parenchymal cells show a loss of iron stores (Figure 4B), and iron levels in the liver of Pfn2-null

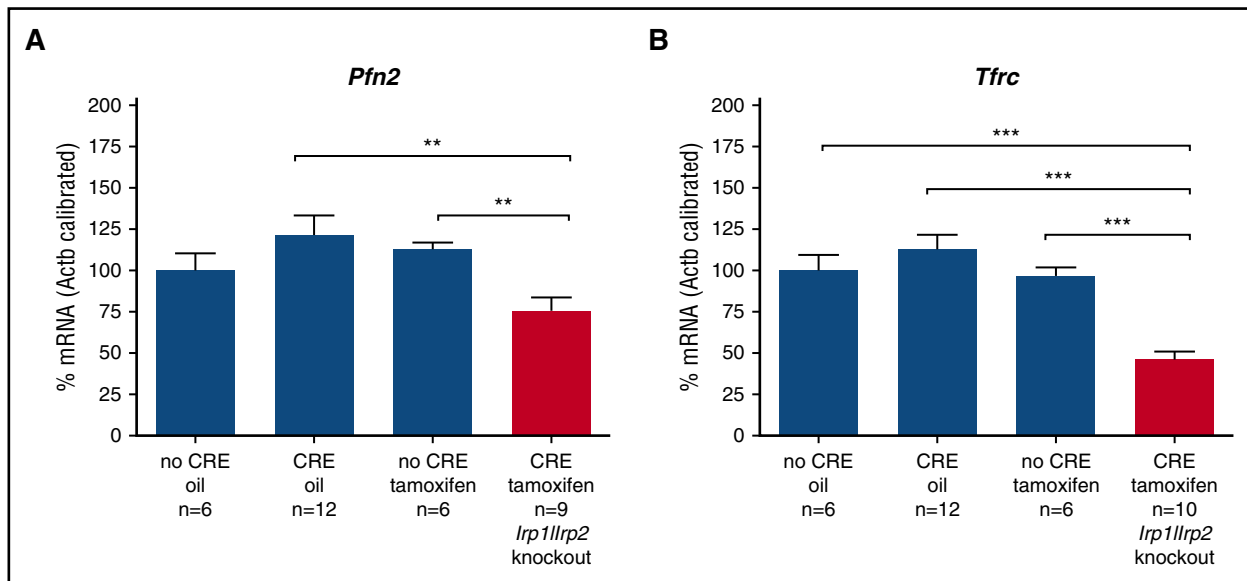


**Figure 2.** Duodenal expression levels of *Pfn2* mRNA in mice with intestinal IRP1 and IRP2 depletion in adult stage. IRP1 and IRP2 deficiency was obtained using the Cre/LoxP technology in a tamoxifen-inducible system in the intestinal mucosa. Adult animals carrying floxed IRP alleles plus the Cre-ERT (XerC recombinase fused to an estrogen receptor tamoxifen-activated) transgene were given tamoxifen (1 mg intraperitoneally per animal per day on 5 consecutive days) to trigger IRP ablation in the intestine. Mice were euthanized 5 weeks after the last tamoxifen injection and *Pfn2* mRNA levels (A) as well as *Tfr* mRNA levels (B) were assessed by qPCR. Control mice (blue bars) were WT mice treated with oil (no CRE oil) or tamoxifen (no CRE tamoxifen), or CRE-expressing mice receiving the vehicle only (CRE oil). *Tfr* mRNA expression was assessed as a molecular signature of IRP deficiency. The histograms represent mRNA levels after calibration to  $\beta$ -actin and normalization to the “no Cre oil” control. *P* values were determined by unpaired 2-tailed Student *t* test, \*\**P* ≤ .01, \*\*\**P* ≤ .001.

animals were reduced by 40% (Figure 4C). Similar results were obtained in 2- to 3-week-old mice (data not shown), indicating that liver iron depletion occurs early in life. Depletion of the liver iron store was not due to increased urinary iron excretion (supplemental Figure 6) and was not associated with any hematological abnormality nor with any alteration of serum iron parameters (supplemental Table 2).

Together, these results show that *Pfn2* plays an important role in brain and liver iron metabolism.

#### Brain iron accumulation in *Pfn2*<sup>-/-</sup> mice

Total iron was selectively increased in the olfactory bulb, hippocampus, and midbrain of 7- to 9-month-old *Pfn2*<sup>-/-</sup> mice, the 3 areas where *Pfn2* expression levels are highest (C. Liemersdorf, I. D. Ozer, A. Husch, W.W., and P.P.B., manuscript in preparation), but was unchanged in other brain regions, such as striatum, cortex, and cerebellum (Figure 4E).

Despite iron loading, ferritin protein levels in hippocampus were reduced (Figure 5A), with no concomitant change in *Fth1* and *Ftl* mRNA levels (Figure 5B). TEM in the hippocampus of *Pfn2*-deficient mice revealed abnormal electron-dense aggregates inside a subset of membrane organelles that resemble mitochondria, as indicated by the presence of lamellae (Figure 5C white arrow). The presence of iron aggregates in hippocampus was confirmed by EDS (Figure 5D). A closer look at these organelles revealed 2 electron-dense structures possibly corresponding to iron deposits: large amorphous biomineral aggregates (Figure 5C arrow 1) and more defined nanoparticles (Figure 5C arrow 2). Both entities are different from the typical iron aggregate present in spleen as ferritin shells (Figure 5C arrow 3) or as hemosiderin (Figure 5C arrow 4). Structurally, both hippocampal iron-containing species (arrow 1 and 2) differ from normal and pathological (observed in neurodegenerative diseases) cytoplasmic ferritins deposits<sup>40,42</sup> and from the mitochondrial biomineral iron aggregates found in the heart of Friedreich ataxia mice.<sup>43</sup>

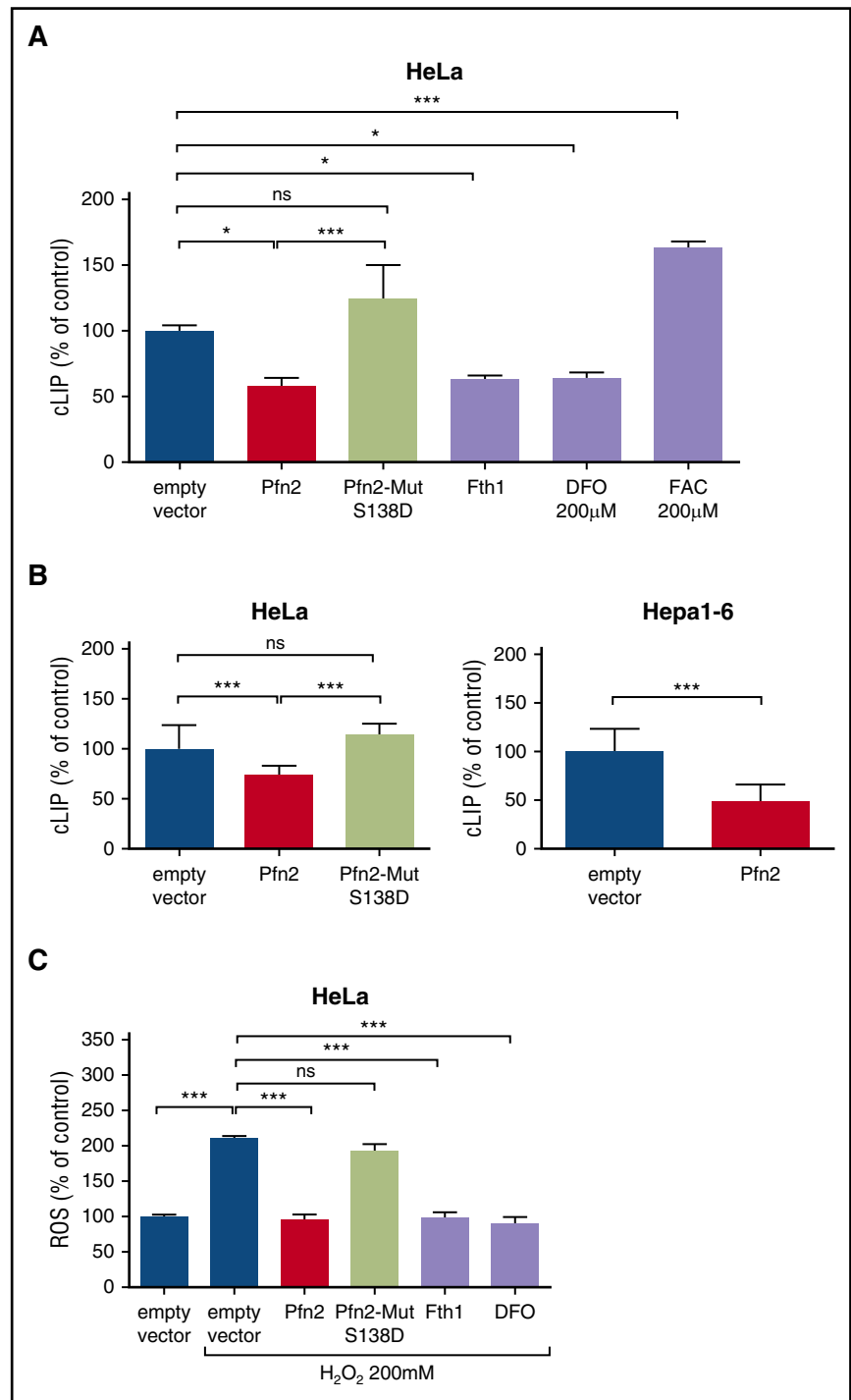
#### Hepatic iron metabolism in *Pfn2*<sup>-/-</sup> mice

The decrease of liver iron content in *Pfn2*<sup>-/-</sup> mice was accompanied by a significant reduction of ferritin L expression at both the protein (Figure 6A) and the mRNA level (Figure 6C). In line with the decreased hepatic iron content, *Bmp6* mRNA expression in *Pfn2*<sup>-/-</sup> livers was reduced by 30% (Figure 6C). Although the reduction of the liver iron content and the concomitant suppression of *Bmp6* would predict a decrease in hepcidin expression, hepatic *Hamp1* mRNA levels remain unchanged in *Pfn2*<sup>-/-</sup> mice (Figure 6C). We hypothesized that antagonistic cues such as inflammation<sup>44</sup> could counteract the regulation of *Hamp1* by low iron in *Pfn2*<sup>-/-</sup> animals. Indeed, expression array analysis of *Pfn2*<sup>-/-</sup> livers (supplemental Table 3) revealed a mild activation of the Il6 pathway (activation z score: 0.247) associated with the upregulation of several Il6-target genes (supplemental Table 4). In line with this observation, plasma Il6 concentration was found to be elevated in *Pfn2*<sup>-/-</sup> animals (Figure 6B). Furthermore, *Pfn2*-deficient mice displayed a tendency for increased expression of several proinflammatory cytokine mRNAs in the liver, including *Saal*, *Tnfa*, *ActivinB*, *Il1β*, and *Il6* (Figure 6C). Thus, the failure to downregulate *Hamp1* in *Pfn2*<sup>-/-</sup> animals with low hepatic iron stores could be explained by concomitant stimulation of the gene's transcription under mild proinflammatory conditions.

Our expression array analysis overall showed 20 upregulated and 29 downregulated genes in the liver of *Pfn2*<sup>-/-</sup> mice compared with control littermates (representing 0.06% and 0.08%, respectively, of the tested transcriptome) (supplemental Table 4). *Lipocalin 2*, an iron-trafficking protein that mediates the uptake of siderophores and catechol-Fe(III) complexes,<sup>45,46</sup> was among the upregulated genes and its increase was confirmed by qPCR (Figure 6C).

Iron uptake in liver is also dependent on *Dmt1*, which is encoded by the *Slc11a2* gene.<sup>1</sup> We analyzed the expression of the *Slc11a2*-IRE and non-IRE mRNA isoforms<sup>47</sup> by qPCR. We observed a statistically

**Figure 3. LIP and ROS levels in cell lines overexpressing Pfn2.** (A) HeLa cells were transiently transfected with pCMV6-Kan/Neo empty vector, pCMV6-Pfn2, or Pfn2-Mut S138D vector. As control, cells were transfected with pCMV6-Fth1 vector or with the empty vector and treated with 200  $\mu$ M DFO or 200  $\mu$ M ferric ammonium citrate (FAC) for 16 hours. cLIP was measured by the calcein-AM method 48 hours after transfection. Data were normalized to cells transfected with the empty vector, set as 100%. Means  $\pm$  standard deviation (SD) are shown. (B) Stable Hepa1-6 and HeLa clones overexpressing the WT mouse Pfn2 or Pfn2-Mut S138D were isolated, and LIP was measured and normalized to cells stably transfected with the pCMV6 empty vector, set as 100%. Means  $\pm$  SD are shown. (C) ROS levels were measured using the 2',7'-dichlorofluorescein diacetate method in HeLa cells transiently transfected with pCMV6-Kan/Neo empty vector, pCMV6-Pfn2, Pfn2-Mut S138D, or pCMV6-Fth1 vectors or in cells transfected with the empty vectors and treated with 200  $\mu$ M DFO for 16 hours. ROS levels were assayed 48 hours after transfection following a pretreatment with 200  $\mu$ M H<sub>2</sub>O<sub>2</sub> to induce ROS generation. ROS quantifications were normalized to cells transfected with the empty vector and not treated with H<sub>2</sub>O<sub>2</sub>, set as 100%. Means  $\pm$  SD are shown. \* $P \leq .05$ , \*\*\* $P \leq .001$ . ns, not significant.



significant and specific upregulation of the *Slc11a2*-IRE mRNA isoform in *Pfn2*<sup>-/-</sup> liver samples (Figure 6C), which could possibly be due to increased IRP binding to the *Slc11a2*-IRE mRNA under iron-deficient conditions.

#### Spleen iron metabolism in *Pfn2*<sup>-/-</sup> mice

Spleen non-heme size and iron content were comparable between *Pfn2*<sup>-/-</sup> mice and control mice (Figure 4C; supplemental Figure 7A). No evidence of extramedullary hematopoiesis was detected in *Pfn2*<sup>-/-</sup> mice (supplemental Figure 7B-C). Splenic

structural iron deposits studied by TEM were expectedly present in lysosome-like structures arranged in  $\approx$ 5-nm large electron-dense nanoparticles (corresponding to the ferritin iron cores) that are usually described as hemosiderin (Figure 5C arrow 4). Accordingly, ferritin L and H mRNA and protein levels were not changed (Figure 6E and data not shown). However, we detected a statistically significant increase in ferroportin protein and RNA level in the spleen of *Pfn2*<sup>-/-</sup> mice (Figure 6D-E), which could serve as a means to counterbalance the effect of inappropriately normal hepcidin levels on ferroportin membrane expression.



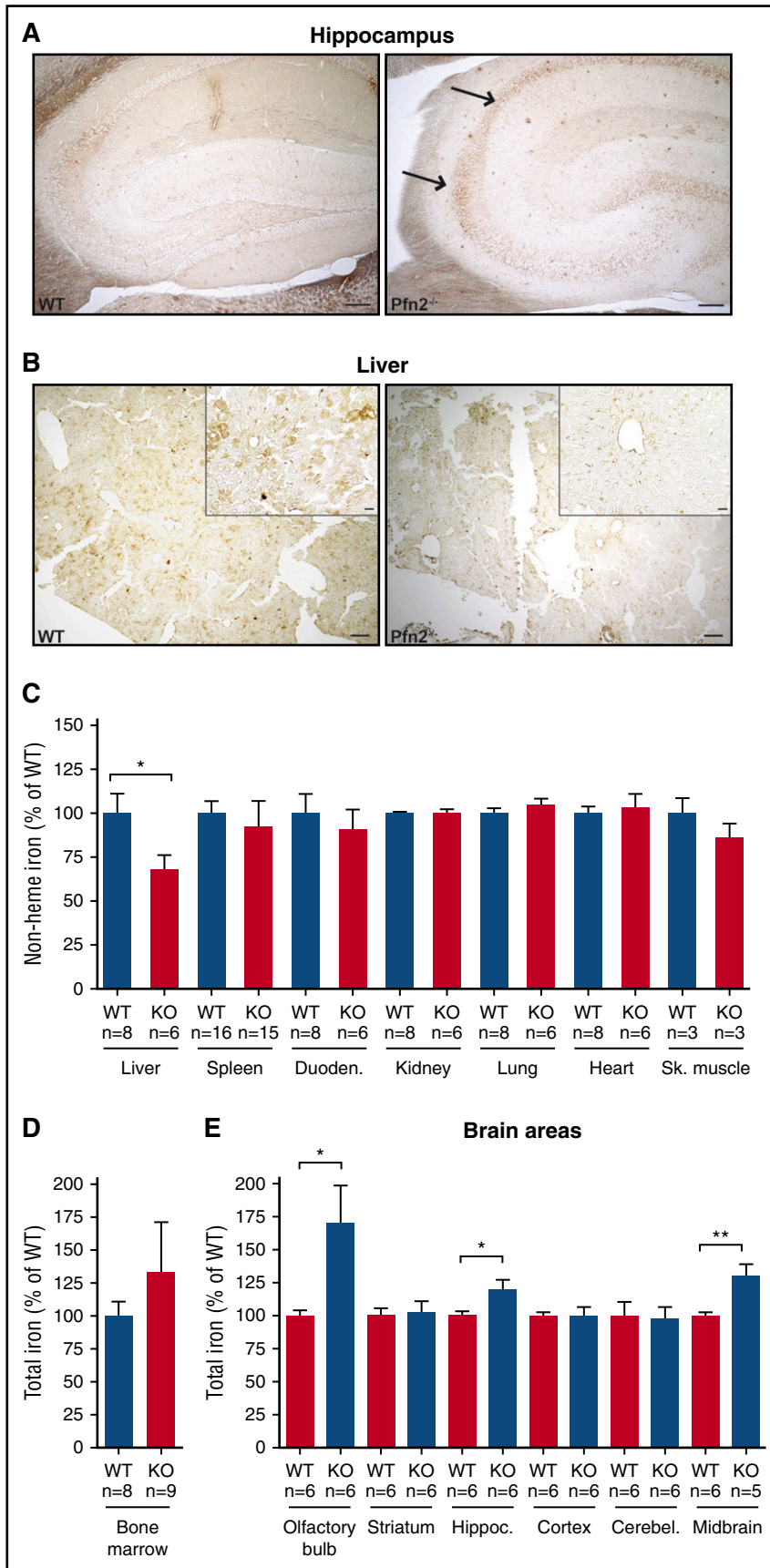


**Figure 4. Abnormal iron distribution in *Pfn2*<sup>-/-</sup> vs WT mice.** Enhanced Prussian blue staining in brain (A) and liver (B) of Perls-perfused *Pfn2*<sup>-/-</sup> and WT mice. In the *Pfn2*<sup>-/-</sup> brain section, the arrows point to CA1-CA2 hippocampal regions, enriched in iron. In contrast, iron is lost in liver parenchymal cells. Scale is 100  $\mu$ m in panel A, and 200  $\mu$ m in low-magnification panels and 20  $\mu$ m in the high-magnification insets in panel B. (C) Tissue non-heme iron content measured using the bathophenanthroline chromogen method in the indicated tissues shows a loss of 40% of iron in the liver of *Pfn2*<sup>-/-</sup> mice. Total iron content measured by atomic absorption method in bone marrow (D) and brain areas (E) shows iron overload in olfactory bulbs, hippocampus, and midbrain of *Pfn2*<sup>-/-</sup> mice. Measures are given as percentage of control WT littermates. The sample size (n) is indicated. P values were determined by unpaired 2-tailed Student t test, \* $P \leq .05$ , \*\* $P \leq .01$ .

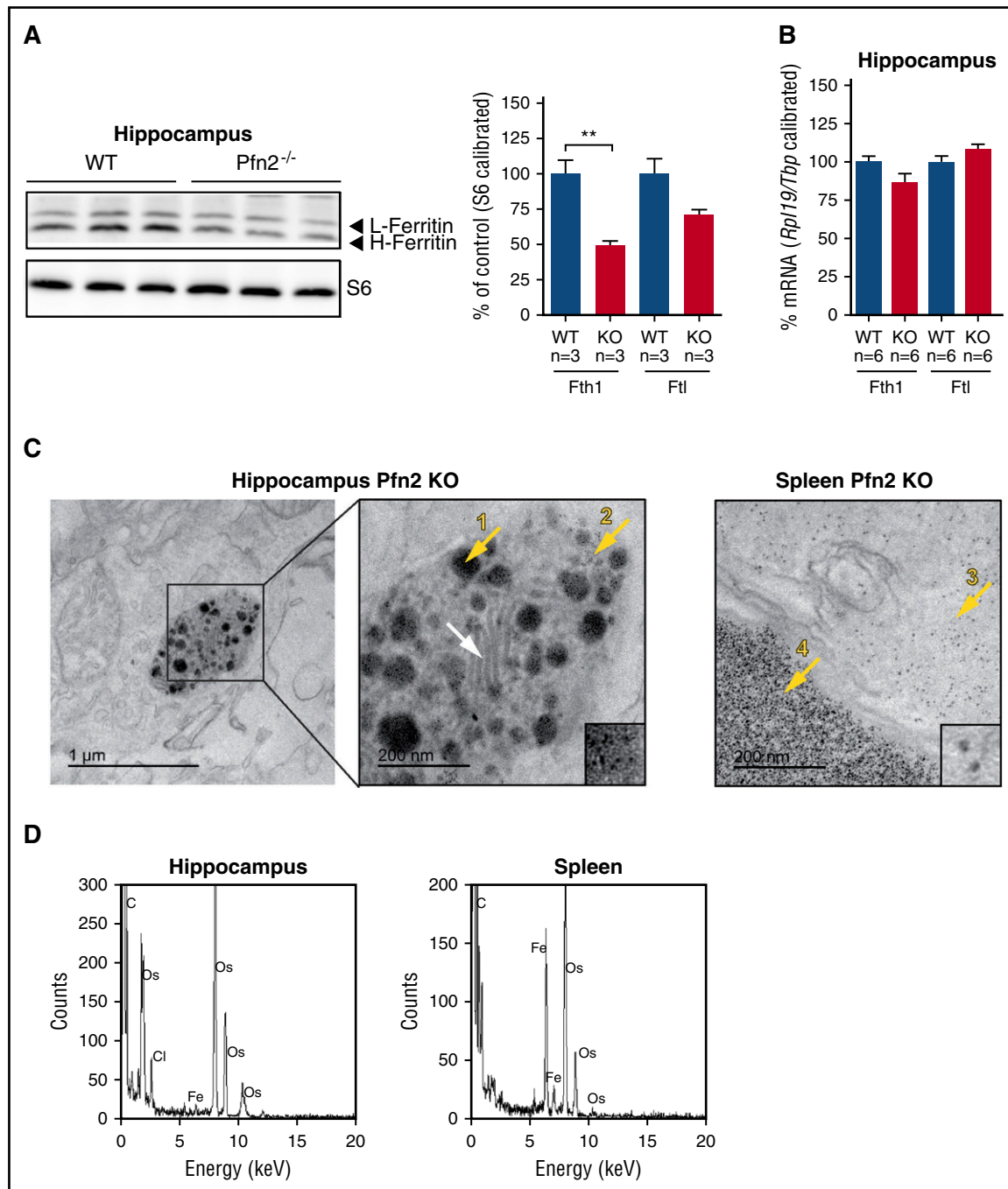


**Figure 5. Ferritin L and H protein and mRNA levels and iron deposits in the hippocampus of *Pfn2*<sup>-/-</sup> mice.** (A) Hippocampal ferritin L (Ftl) and ferritin H (Fth1) protein measured by western blotting are reduced in *Pfn2* KO mice compared with WT controls. Ribosomal protein S6 levels were used for calibration. Graphs represent quantified data normalized to the WT control (set as 100%). Sample size (n) is indicated. (B) Hippocampal ferritin L (*Ftl*) and ferritin H (*Fth1*) mRNA levels measured by qPCR show no difference between *Pfn2*<sup>-/-</sup> and WT control mice. mRNA expression was calibrated with ribosomal protein L19 (*Rpl19*) and TATA box binding protein (*Tbp*) mRNA expression and normalized to WT mice (set as 100%). Sample size (n) is indicated. (C) On the left side, TEM sample image from the hippocampus of a *Pfn2*<sup>-/-</sup> mouse. The boxed area is magnified on its right. On the right side, sample image from the spleen of a *Pfn2*<sup>-/-</sup> mouse. TEM images of hippocampus (second image) and spleen (third image from left) are at the same magnification for comparison of the aggregates size and morphology. Lamellae structures characterizing a mitochondrion are highlighted by a white arrow. Iron aggregates of different morphologies are indicated by yellow arrows: mitochondrial amorphous and big clustered aggregates (1), isolated biomineral nanoparticles (2), cytoplasm dispersed ferritin cores (3), and spleen hemosiderin aggregates (4). Small insets from center and right TEM images are at the same magnification, showing the smaller particle size observed in hippocampus (2) in comparison with the spleen ferritin cores (3). (D) In the hippocampus and spleen of *Pfn2*<sup>-/-</sup> mice, electron-dense areas have been tested by EDS to confirm the presence of iron. \*\**P* ≤ .01.

## Discussion

IRP-mutant mouse models revealed that the IRP/IRE regulatory system is critical for securing physiological iron distribution between major

sites of systemic iron homeostasis. Here, we describe a new IRP mRNA target, *Pfn2*, and unveil a novel function for this actin-binding protein in iron metabolism.

We show that *Pfn2* mRNA harbors a conserved and functional IRE in its 3' UTR. Similar to the well-characterized



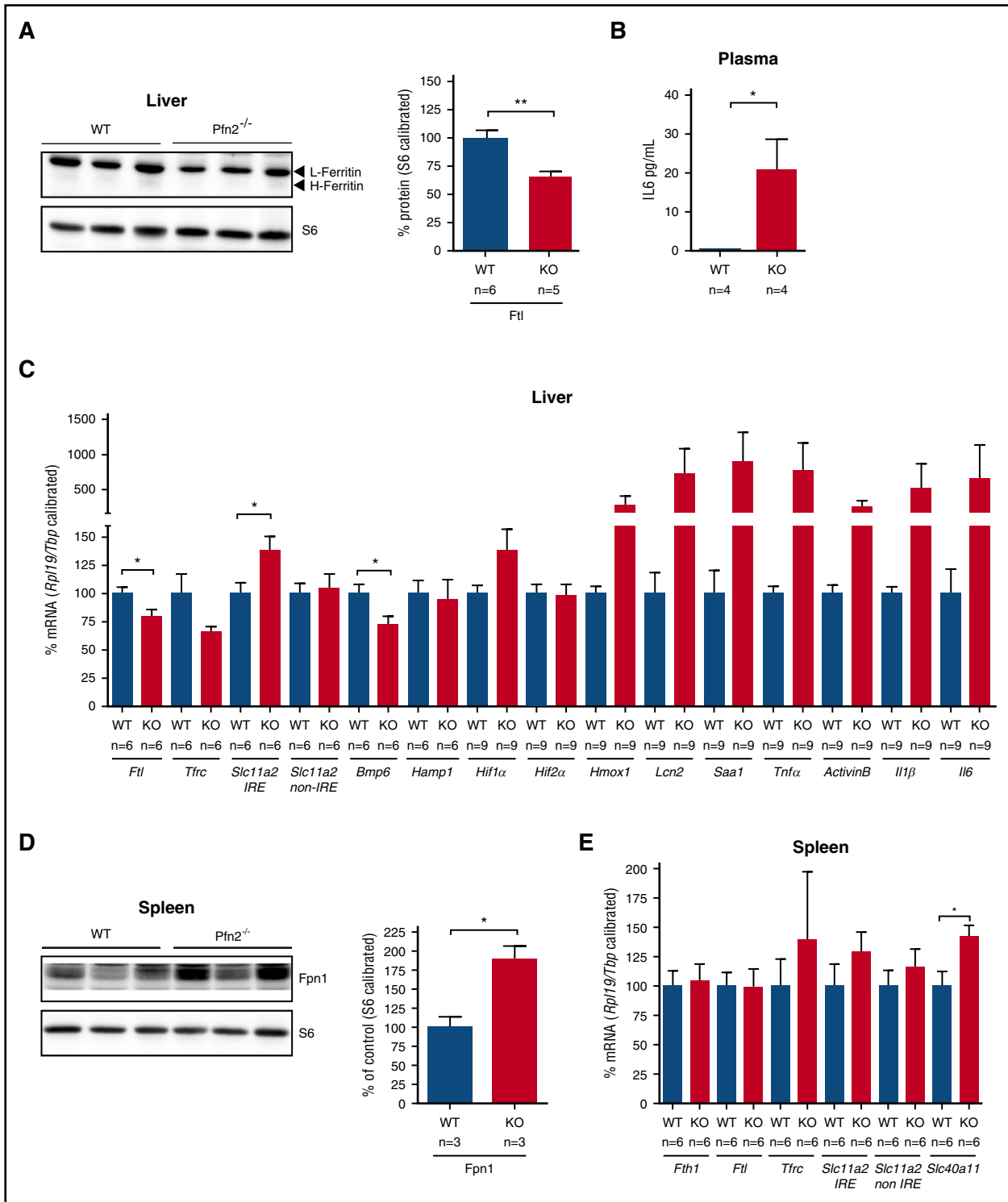


**Figure 6. Protein and RNA levels of iron-related genes in liver and spleen of *Pfn2*<sup>-/-</sup> and WT mice.** Liver (A) ferritin L and ferritin H protein levels measured by western blotting are reduced in *Pfn2*<sup>-/-</sup> mice compared with WT controls, whereas splenic (D) ferroportin protein levels are increased in *Pfn2*<sup>-/-</sup> mice compared with WT controls. Ribosomal protein S6 levels were used for calibration. Graphs represent quantified data normalized to the WT sample (set as 100%). Samples size (n) is indicated. RNA expression of iron-related genes was analyzed by qPCR in liver (C) and spleen (E). mRNA expression was calibrated with *Fpl19* and *Tbp* mRNA expression and normalized to WT mice (set as 100%). Sample size (n) is indicated. (B) Plasma levels of IL6 were measured by Luminex immunoassay. *Bmp6*, bone morphogenetic protein 6; *Hamp1*, hepcidin; *Hif1α/2α*, hypoxia inducible factor 1α/2α; *Hmox1*, heme oxygenase 1; *Il1β/6*, interleukin 1β/6; *Lcn2*, lipocalin 2; *Saa1*, serum amyloid A1; *Slc40a11*, ferroportin (protein: Fpn1); *Tnfα*, tumor necrosis factor α. \**P* ≤ .05, \*\**P* ≤ .01.

3' IRE-containing *Tfrc* mRNA, *Pfn2* transcript levels are reduced upon IRP ablation in vivo in mice. Nevertheless, steady-state *Pfn2* mRNA levels are largely unchanged under iron-deficient conditions,

both in cultured cells and in mice. The lack of iron regulation of *Pfn2* is not totally surprising, because it is already known that, for example, the modulation of the *Slc11a2* mRNA by iron is cell-line specific and

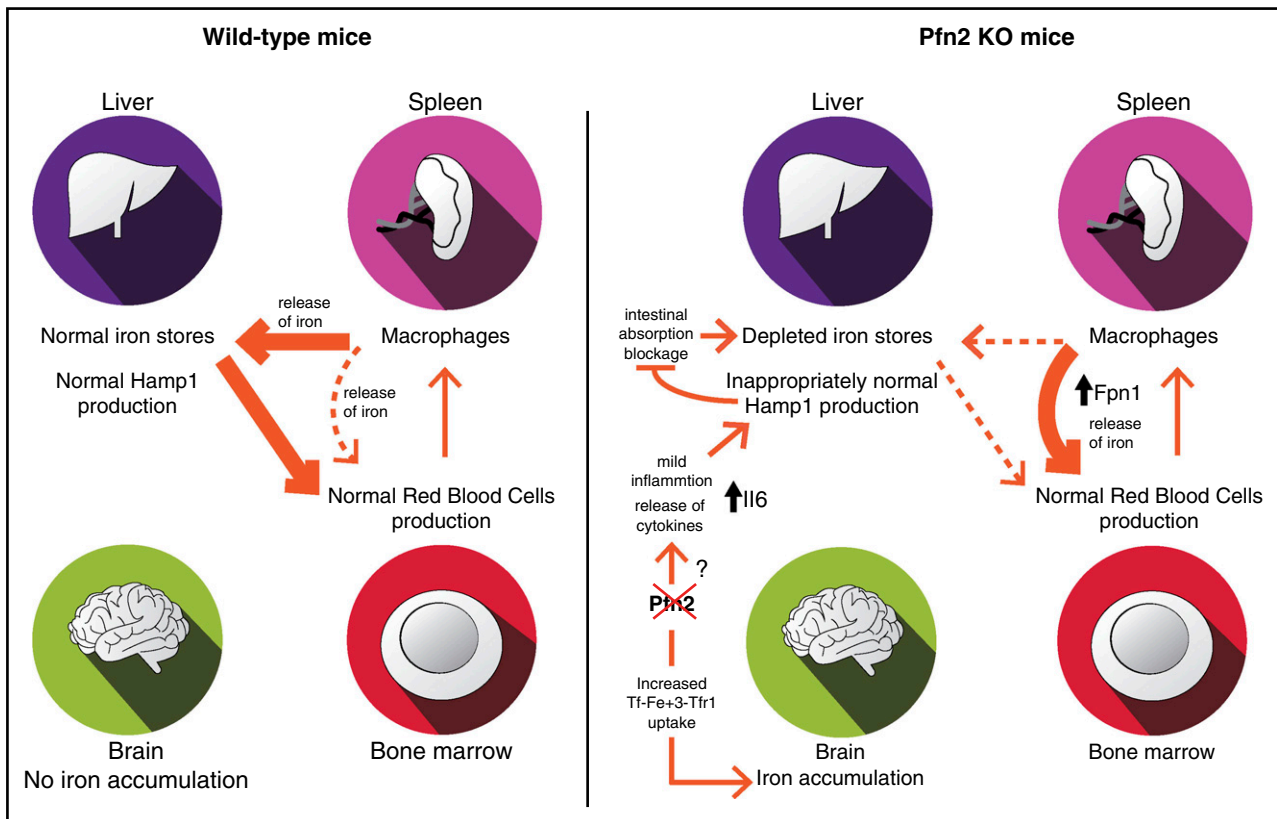


**Figure 7. Model for systemic iron distribution and homeostasis in WT vs *Pfn2*<sup>-/-</sup> mice.** *Pfn2* KO mice exhibit brain iron accumulation and depletion of liver iron stores with normal hematological parameters. Brain iron overload can be attributed to an increase in transferrin-transferrin receptor endocytosis (Tf-Fe<sup>3+</sup>-TfR1) because of the lack of *Pfn2* that negatively regulates this process. Although in WT mice erythropoiesis is supported mainly by liver but also splenic iron, in *Pfn2*<sup>-/-</sup> mice erythropoiesis is supported exclusively by the spleen, where we have detected a substantial increase in ferroportin (*Fpn1*) production. In *Pfn2*<sup>-/-</sup> mice *hepcidin* (*Hamp1*), production in liver is inappropriately normal despite low-iron levels, which should downregulate *hepcidin* production in order to increase dietary iron absorption and restore liver iron content. *Hepcidin* inappropriately normal levels in liver of *Pfn2*<sup>-/-</sup> mice are caused by a mild increase in the release of *Il6* proinflammatory cytokine that can overrule opposite inhibitory signals.

is influenced by the differentiation state of the cell.<sup>4</sup> In addition, multiple integrative and opposing signals contribute to the regulation of several single IRE-containing mRNAs, such as *Epa1* (protein HIF2alpha), *Slc40a1* (protein ferroportin), and *Slc11a2* (protein Dmt1). Overall, it seems that a straightforward regulation of 3' IRE-containing mRNAs by iron levels and IRPs is only consistently observed in the case of *Tfrc*, although even for this transcript the fold regulation is very variable and depends on the cell line or tissue analyzed.

On the other hand, mice with constitutive deficiency of *Pfn2* exhibit a striking iron phenotype, with iron accumulation in specific areas of the brain and a reduction of the liver iron stores, although displaying normal red blood cell counts and plasma iron parameters.

Iron accumulation in the brain of *Pfn2*<sup>-/-</sup> mice correlates with the expression pattern of *Pfn2*, being the highest in hippocampus, olfactory bulb, and midbrain (C. Liemersdorf, I. D. Ozer, A. Husch, W.W., and P.P.B., manuscript in preparation). It is well established that iron bound to transferrin is internalized through receptor-mediated endocytosis of TfR1, involving clathrin-coated pits and Dnm1.<sup>48</sup> *Pfn2* interacts with and sequesters Dnm1 in neurons, thereby preventing its binding to endocytic effectors.<sup>23</sup> Thus, *Pfn2* acts as a negative regulator of endocytosis. Indeed, neurons from *Pfn2*-KO mice show increased endocytic rate, and ectopic overexpression of *Pfn2* in HeLa cells slows down transferrin uptake.<sup>23</sup> In this work, we observed that *Pfn2* overexpression in several cell lines decreased the cLIP. Hence, it is conceivable that the iron overload in the brain of *Pfn2*<sup>-/-</sup> mice is due to an increased rate of transferrin-TfR1 endocytosis in the absence of *Pfn2* (Figure 7). Interestingly, we show that iron accumulation in

the hippocampus of *Pfn2*<sup>-/-</sup> mice occurs in previously undescribed biomineral iron forms inside organelles, whose membrane structure resembles mitochondria. As *Pfn2*<sup>-/-</sup> mice do not manifest overt neurodegeneration or ataxia, we hypothesize that the iron aggregates could be a harmless way to confine the otherwise highly toxic iron excess inside the neurons.

Although iron accumulates in the brain of *Pfn2*<sup>-/-</sup> mice, we were surprised to observe a substantial depletion of the liver iron stores. Although microarray data did not reveal major alterations in this tissue, we observed upregulation of genes involved in liver uptake of extracellular iron that could likely be a compensatory mechanism to reestablish hepatic iron stores. The liver iron content of *Pfn2*-null mice is deficient in the context of unchanged spleen and duodenal iron levels as well as normal red blood cell counts and serum iron parameters. Hence, it cannot be explained by the classical mobilization of the hepatic iron stores in conditions of anemia. Future work is needed to elucidate this phenomenon.

Our hepatic expression analysis revealed a contradictory situation in low-iron-stores condition: *Bmp6* levels were low, whereas *Hamp1* transcript levels were not decreased. Our microarray and qPCR data in liver and our plasma *Il6* measurements indicate a mild chronic systemic inflammation in *Pfn2*<sup>-/-</sup> mice. As the absence of *Pfn2* is known to increase neurotransmitter release,<sup>24</sup> it is possible that it affects similarly the release of cytokines produced in different tissues. Therefore, the observed reduction in hepatic *Bmp6* mRNA expression and the increased levels of *Il6* may act as antagonistic signals, maintaining an overall stable *Hamp1* expression.

Spleen non-heme iron content and size were found unchanged in *Pfn2*<sup>-/-</sup> mice. Nevertheless, ferroportin expression was increased in spleens of *Pfn2*<sup>-/-</sup> mice. Because hepcidin negatively regulates membrane ferroportin levels, it is conceivable that increased ferroportin expression in spleen serves to stabilize its membrane presence in order to compensate hepatic iron deficiencies and sustain hematopoiesis, as *Pfn2*<sup>-/-</sup> mice are not anemic (Figure 7).

Our work highlights that altering the expression of a key regulator of membrane trafficking and endocytosis pathways such as Pfn2 alters iron metabolism at the cellular level and affects body iron homeostasis, similarly to defects in other endosomal sorting proteins, such as Snx3,<sup>49</sup> or Sec151.<sup>50</sup> In summary, our studies indicate that Pfn2 is a previously unrecognized critical player in iron homeostasis, which could contribute to human disorders of iron metabolism.

## Acknowledgments

The authors thank Dunja Ferring-Appel for excellent technical assistance with serum iron parameter measurements, Anke Carstensen from the Institut für Klinische Chemie und Klinische Pharmakologie, Universitätsklinikum Bonn for performing the blood analyses on the mice, Lara Nonell from the Microarray Analysis Service of the Hospital del Mar Medical Research Institute for support with microarray analysis, and Mar Mallo and Francesc Sole from the Affymetrix Microarray Platform of the Josep Carreras Leukaemia Research Institute for microarray performance. The authors acknowledge the facilities and the scientific and technical assistance of Cristina Patiño, Rocío San Andrés, and Javier Bueno from the TEM service at Centro Nacional de Biotecnología and M. Puerto Morales from Instituto de Ciencia de Materiales de Madrid, Madrid, Spain for continuous support.

This work was supported by grant SAF2015-70412-R from the Spanish Secretary of Research, Development, and Innovation (Ministerio de Economía, Industria y Competitividad [MINECO]) and grant DJCLS R14/04 from Deutsche José Carreras Leukämie Stiftung, grant 2014 SGR225 (Grups de Recerca Emergent, from

Generalitat de Catalunya) from Generalitat de Catalunya, and financial support from Fundació Internacional Josep Carreras and from Obra Social “la Caixa” Spain (M. Sanchez). All work on the Pfn2 KO mouse model was supported by the Deutsche Forschungsgemeinschaft grant SFB1089 and SPP1464 (W.W.). S.L. was supported by the EMBO Short Term Fellowship ASTF 301-2013 for her work on the *Pfn2*<sup>-/-</sup> mice at the Institute of Genetics, University of Bonn, Bonn, Germany.

## Authorship

Contribution: M. Sanchez and P.P.B. designed and performed research, analyzed the data, and wrote the manuscript; L.G. and B.G. provided reagents and samples, analyzed the data, and wrote the manuscript; M.W.H. and W.W. provided reagents and analyzed the data; and S.L., L.G., M. Shvartsman, M.R., J.C., and A.D.P. performed research and analyzed the data.

Conflict-of-interest disclosure: The authors declare no competing financial interests.

The current affiliation for L.G. is Analytical Chemistry Department, Institute of Nanoscience of Aragon, Universidad de Zaragoza, Zaragoza, Spain.

The current affiliation for M. Shvartsman is European Molecular Biology Laboratory, Monterotondo, Italy.

ORCID profiles: S.L., 0000-0002-3800-1303; B.G., 0000-0002-0501-6357; L.G., 0000-0003-2366-3598; M.R., 0000-0002-6941-1356; J.C., 0000-0001-9268-1672; M.W.H., 0000-0002-4023-7876; P.P.B., 0000-0002-7535-4802; M.S., 0000-0002-6499-5989.

Correspondence: Mayka Sanchez, Josep Carreras Leukaemia Research Institute, Campus ICO–Germans Trias i Pujol, Crta Can Ruti Cami de les Escoles s/n, Badalona, 08916 Spain; e-mail: msanchez@carrerasresearch.org; and Pietro Pilo Boyl, Institute of Genetics, University of Bonn, Karlrobert-Kreiten-Str 13, 53115 Bonn, Germany; e-mail: pietro.piloboyl@uni-bonn.de.

## References

- Hentze MW, Muckenthaler MU, Galy B, Camaschella C. Two to tango: regulation of mammalian iron metabolism. *Cell*. 2010;142(1):24-38.
- Anderson CP, Shen M, Eisenstein RS, Leibold EA. Mammalian iron metabolism and its control by iron regulatory proteins. *Biochim Biophys Acta*. 2012;1823(9):1468-1483.
- Sanchez M, Galy B, Muckenthaler MU, Hentze MW. Iron-regulatory proteins limit hypoxia-inducible factor-2 $\alpha$  expression in iron deficiency. *Nat Struct Mol Biol*. 2007;14(5):420-426.
- Gunshin H, Allerson CR, Polycarpou-Schwarz M, et al. Iron-dependent regulation of the divalent metal ion transporter. *FEBS Lett*. 2001;509(2):309-316.
- McKie AT, Marciani P, Rolfs A, et al. A novel duodenal iron-regulated transporter, IREG1, implicated in the basolateral transfer of iron to the circulation. *Mol Cell*. 2000;5(2):299-309.
- Walden WE, Selezneva AI, Dupuy J, et al. Structure of dual function iron regulatory protein 1 complexed with ferritin IRE-RNA. *Science*. 2006;314(5807):1903-1908.
- Wilkinson N, Pantopoulos K. The IRP/IRE system in vivo: insights from mouse models. *Front Pharmacol*. 2014;5:176.
- Joshi RS, Moran E, Sanchez M. Cellular iron metabolism—the IRP/IRE regulatory network. In: Sarika Arora, ed. *Iron Metabolism*. Rijeka, Croatia: InTech; 2012.
- Yoshinaga M, Nakatsuka Y, Vandenbon A, et al. Regnase-1 maintains iron homeostasis via the degradation of transferrin receptor 1 and prolyl-hydroxylase-domain-containing protein 3 mRNAs. *Cell Reports*. 2017;19(8):1614-1630.
- Galy B, Ferring D, Hentze MW. Generation of conditional alleles of the murine Iron Regulatory Protein (IRP)-1 and -2 genes. *Genesis*. 2005;43(4):181-188.
- Smith SR, Ghosh MC, Ollivierre-Wilson H, Hang Tong W, Rouault TA. Complete loss of iron regulatory proteins 1 and 2 prevents viability of murine zygotes beyond the blastocyst stage of embryonic development. *Blood Cells Mol Dis*. 2006;36(2):283-287.
- Galy B, Ferring-Appel D, Becker C, et al. Iron regulatory proteins control a mucosal block to intestinal iron absorption. *Cell Reports*. 2013;3(3):844-857.
- Galy B, Ferring-Appel D, Kaden S, Gröne HJ, Hentze MW. Iron regulatory proteins are essential for intestinal function and control key iron absorption molecules in the duodenum. *Cell Metab*. 2008;7(1):79-85.
- Galy B, Ferring-Appel D, Sauer SW, et al. Iron regulatory proteins secure mitochondrial iron sufficiency and function. *Cell Metab*. 2010;12(2):194-201.
- Nairz M, Ferring-Appel D, Casarrubea D, et al. Iron regulatory proteins mediate host resistance to salmonella infection. *Cell Host Microbe*. 2015;18(2):254-261.
- Moroishi T, Nishiyama M, Takeda Y, Iwai K, Nakayama KI. The FBXL5-IRP2 axis is integral to control of iron metabolism in vivo. *Cell Metab*. 2011;14(3):339-351.
- Casarrubea D, Viatte L, Hallas T, et al. Abnormal body iron distribution and erythropoiesis in a novel mouse model with inducible gain of iron regulatory protein (IRP)-1 function. *J Mol Med (Berl)*. 2013;91(7):871-881.
- Sanchez M, Galy B, Schwanhäusser B, et al. Iron regulatory protein-1 and -2: transcriptome-wide definition of binding mRNAs and shaping of the cellular proteome by iron regulatory proteins. *Blood*. 2011;118(22):e168-e179.

19. Witke W. The role of profilin complexes in cell motility and other cellular processes. *Trends Cell Biol.* 2004;14(8):461-469.
20. Damke H, Binns DD, Ueda H, Schmid SL, Baba T. Dynamin GTPase domain mutants block endocytic vesicle formation at morphologically distinct stages. *Mol Biol Cell.* 2001;12(9):2578-2589.
21. Ferguson SM, Brasnjo G, Hayashi M, et al. A selective activity-dependent requirement for dynamin 1 in synaptic vesicle endocytosis. *Science.* 2007;316(5824):570-574.
22. Witke W, Podtelejnikov AV, Di Nardo A, et al. In mouse brain profilin I and profilin II associate with regulators of the endocytic pathway and actin assembly. *EMBO J.* 1998;17(4):967-976.
23. Gareus R, Di Nardo A, Rybin V, Witke W. Mouse profilin 2 regulates endocytosis and competes with SH3 ligand binding to dynamin 1. *J Biol Chem.* 2006;281(5):2803-2811.
24. Pilo Boyl P, Di Nardo A, Mulle C, et al. Profilin2 contributes to synaptic vesicle exocytosis, neuronal excitability, and novelty-seeking behavior. *EMBO J.* 2007;26(12):2991-3002.
25. Gray NK, Quick S, Goossen B, et al. Recombinant iron-regulatory factor functions as an iron-responsive-element-binding protein, a translational repressor and an aconitase. A functional assay for translational repression and direct demonstration of the iron switch. *Eur J Biochem.* 1993;218(2):657-667.
26. Sanchez M, Galy B, Dandekar T, et al. Iron regulation and the cell cycle: identification of an iron-responsive element in the 3'-untranslated region of human cell division cycle 14A mRNA by a refined microarray-based screening strategy. *J Biol Chem.* 2006;281(32):22865-22874.
27. Lusciati S, Tolle G, Aranda J, et al. Novel mutations in the ferritin-L iron-responsive element that only mildly impair IRP binding cause hereditary hyperferritinaemia cataract syndrome. *Orphanet J Rare Dis.* 2013;8:30.
28. Liu Z, Lanford R, Mueller S, et al. Siderophore-mediated iron trafficking in humans is regulated by iron. *J Mol Med (Berl).* 2012;90(10):1209-1221.
29. Epsztejn S, Kakhlon O, Glickstein H, Breuer W, Cabantchik I. Fluorescence analysis of the labile iron pool of mammalian cells. *Anal Biochem.* 1997;248(1):31-40.
30. Santamaria R, Irace C, Festa M, Maffettone C, Colonna A. Induction of ferritin expression by oxalomalate. *Biochim Biophys Acta.* 2004; 1691(2-3):151-159.
31. Torrance JD, Bothwell TH. A simple technique for measuring storage iron concentrations in formalinised liver samples. *S Afr J Med Sci.* 1968; 33(1):9-11.
32. Patel BN, Dunn RJ, Jeong SY, Zhu Q, Julien JP, David S. Ceruloplasmin regulates iron levels in the CNS and prevents free radical injury. *J Neurosci.* 2002;22(15):6578-6586.
33. Gutiérrez L, Quintana C, Patiño C, et al. Iron speciation study in Hfe knockout mice tissues: magnetic and ultrastructural characterisation. *Biochim Biophys Acta.* 2009;1792(6):541-547.
34. Meguro R, Asano Y, Iwatsuki H, Shoumura K. Perfusion-Perls and -Turnbull methods supplemented by DAB intensification for nonheme iron histochemistry: demonstration of the superior sensitivity of the methods in the liver, spleen, and stomach of the rat. *Histochem Cell Biol.* 2003; 120(1):73-82.
35. Rodrigues PN, Gomes SS, Neves JV, et al. Mycobacteria-induced anaemia revisited: a molecular approach reveals the involvement of NRAMP1 and lipocalin-2, but not of hepcidin. *Immunobiology.* 2011;216(10):1127-1134.
36. Smyth GK. Linear models and empirical bayes methods for assessing differential expression in microarray experiments. *Stat Appl Genet Mol Biol.* 2004;3:3.
37. Benjamini Y, Hochberg Y. Controlling the false discovery rate: a practical and powerful approach to multiple testing. *J R Stat Soc Series B.* 1995; 57(1):289-300.
38. Sanchez M, Galy B, Hentze MW, Muckenthaler MU. Identification of target mRNAs of regulatory RNA-binding proteins using mRNP immunopurification and microarrays. *Nat Protoc.* 2007;2(8):2033-2042.
39. Campillos M, Cases I, Hentze MW, Sanchez M. SIREs: searching for iron-responsive elements. *Nucleic Acids Res.* 2010;38(Web Server issue): W360-367.
40. Di Nardo A, Gareus R, Kwiatkowski D, Witke W. Alternative splicing of the mouse profilin II gene generates functionally different profilin isoforms. *J Cell Sci.* 2000;113(Pt 21):3795-3803.
41. Lambrechts A, Braun A, Jonckheere V, et al. Profilin II is alternatively spliced, resulting in profilin isoforms that are differentially expressed and have distinct biochemical properties. *Mol Cell Biol.* 2000;20(21):8209-8219.
42. Quintana C, Gutiérrez L. Could a dysfunction of ferritin be a determinant factor in the aetiology of some neurodegenerative diseases? *Biochim Biophys Acta.* 2010;1800(8):770-782.
43. Whitnall M, Suryo Rahmanto Y, Huang ML, et al. Identification of nonferritin mitochondrial iron deposits in a mouse model of Friedreich ataxia. *Proc Natl Acad Sci USA.* 2012;109(50): 20590-20595.
44. Nemeth E, Rivera S, Gabayan V, et al. IL-6 mediates hypoferrremia of inflammation by inducing the synthesis of the iron regulatory hormone hepcidin. *J Clin Invest.* 2004;113(9): 1271-1276.
45. Devireddy LR, Gazin C, Zhu X, Green MR. A cell-surface receptor for lipocalin 24p3 selectively mediates apoptosis and iron uptake. *Cell.* 2005; 123(7):1293-1305.
46. Bao G, Clifton M, Hoette TM, et al. Iron traffics in circulation bound to a siderocalin (Ngal)-catechol complex. *Nat Chem Biol.* 2010;6(8):602-609.
47. Hubert N, Hentze MW. Previously uncharacterized isoforms of divalent metal transporter (DMT)-1: implications for regulation and cellular function. *Proc Natl Acad Sci USA.* 2002;99(19):12345-12350.
48. van der Blik AM, Redelmeier TE, Damke H, Tisdale EJ, Meyerowitz EM, Schmid SL. Mutations in human dynamin block an intermediate stage in coated vesicle formation. *J Cell Biol.* 1993;122(3):553-563.
49. Chen C, Garcia-Santos D, Ishikawa Y, et al. Snx3 regulates recycling of the transferrin receptor and iron assimilation. *Cell Metab.* 2013;17(3):343-352.
50. Lim JE, Jin O, Bennett C, et al. A mutation in Sec15l1 causes anemia in hemoglobin deficit (hbd) mice. *Nat Genet.* 2005;37(11):1270-1273.